Resonance Damping and Parameter Design Method for LCL-LC Filter Interfaced Grid-Connected Photovoltaic Inverters

Li, Zipeng; Jiang, Aiting; Shen, Pan; Han, Yang; Guerrero, Josep M.

Resonance Damping and Parameter Design Method for LCL-LC Filter Interfaced Grid-Connected Photovoltaic Inverters

Zipeng Li, Aiting Jiang, Pan Shen, Yang Han
Dept. of Power Electronics, School of Mechatronics Eng.,
University of Electronic Science and Technology of China
Chengdu 611731, China
E-mail: hanyang@uestc.edu.cn

Josep M. Guerrero
Department of Energy Technology
Aalborg University
Aalborg 9220, Denmark
E-mail: joz@et.aau.dk

Abstract—In order to attenuate PWM harmonics effectively and reduce filter cost and volume, LCL-LC filter is proposed using a combination of LCL filter and an LC series resonant part. Compared with LCL filter, LCL-LC filter is characterized with decreased total inductance and better switch-frequency harmonics attenuation ability, but the resonant problem affects the system stability remarkably. In this paper, active damping based on the capacitor voltage feedback is proposed using the concept of the equivalent virtual impedance in parallel with the capacitor. With the consideration of system delay, this paper presents a systematic design method for the LCL-LC filtered grid-connected photovoltaic (PV) system. With this method, controller parameters and the active damping feedback coefficient are easily obtained by specifying the system stability and dynamic performance indices, and it is more convenient to optimize the system performance according to the predefined satisfactory region. Finally, the simulation results are presented to validate the proposed design method and control scheme.

Keywords—active damping; grid-connected photovoltaic (PV) converter; LCL-LC filter; proportional resonant (PR) controller;

I. INTRODUCTION

The increasing global energy consumption has greatly accelerated the demand for renewable energy, such as wind and solar energy, and the grid connected photovoltaic (PV) power generation is growing with the tendency of increased scale and capacity [1-3]. As far as grid-connected photovoltaic (PV) inverters are concerned, the stability analysis and dynamic interaction between PV plants and distribution system are attracting a lot of attention. When the two-level inverters are used, the output voltages are polluted with considerable harmonic components, thus the injected grid currents may contain high-frequency harmonics near the switching frequency caused by the pulse-width modulation (PWM) process. Therefore, a low-pass filter (typical *LCL* filter) must be installed between each PV inverter and the unity for attenuating the high frequency harmonics injected into the point of common coupling (PCC) [4, 5].

The filter can be of different types [6]. Compared with the first order *L* filter, the third-order *LCL* filter can meet the grid code requirements with smaller size and cost, especially for applications above several kilowatts. In [7], a new filter named *LCL-LC* filter is proposed, which is a combination of an *LCL* and an *LC* series resonant circuits and has the ability of attenuating switching frequency harmonics with an attenuation rate of -60 dB/decade. However, *LCL-LC* filter suffers from the resonance problems, two resonant peaks are introduced by *LCL-LC* filter which may cause system instability. Generally, passive damping [5] or active damping [8, 9] methods are adopted for damping the resonance of output filter in PV inverter. Passive damping can be realized by adding passive components in the system [10], a direct way to damp the resonance of the *LCL-LC* filter is to place a damping resistor in series with the filter capacitor [7]. In this way, two resonance peaks are effectively damped, the harmonics attenuation ability in the range of switching frequency is not weaken, but the physical resistors will inevitably lead to higher losses and decreases system efficiency [11].

Therefore, the active damping method is a preferred solution for the residential PV inverters with a higher reliability and reduced power loss. In this paper, a systematic parameters design method for *LCL-LC* filtered grid-connected photovoltaic (PV) system using capacitor voltage feedback scheme is proposed. By using this method, the controller parameters and active damping feedback coefficient can be easily obtained by selecting the reasonable range of system stability and dynamic performance indices, hence it is convenient to optimize the system performance according to the satisfactory region. Further, the active damping scheme for the *LCL-LC* grid-connected PV system based on the capacitor voltage feedback is found to have a strong robustness against the grid impedance variation and the grid voltage fluctuation conditions.

This paper is organized as follows. In section II, the system model and the passive damping methods for *LCL-LC* filter are presented. On this basis, the active damping method based on capacitor current feedback of the *LCL-LC* is presented in section III. In section IV, a systematic controller design method for *LCL-LC* filtered grid-connected photovoltaic (PV)

system is proposed, the design example is also given. In Section V, the simulation results validate the proposed control scheme and the parameter design method. Finally, Section VI concludes this paper.

II. SYSTEM CONFIGURATION AND PASSIVE DAMPING METHODS FOR THE LCL-LC FILTER-BASED PV INVERTERS

Fig. 1(a) shows the main circuit of a two-stage *LCL-LC* filtered grid-connected PV system. The boost DC-DC connected to the PV panels step up the voltage of the DC bus to a proper level for the PV inverter. The H-bridge DC-AC inverter produces PWM sinusoidal current injected into the grid based on the Maximum Power Point Tracking (MPPT) algorithms [12]. The voltages at the PCC are sampled for Phase Locked Loop (PLL), the injected grid current i_g is sensed for current control and the capacitor current u_c is sensed for active damping.

And the corresponding current control circuit is shown in Fig. 1(b), K_{pwm} is the transfer function of PWM inverter, which is defined as V_{dc}/V_{tri}, where V_{dc} is amplitude of the input dc voltage and V_{tri} is the amplitude of the triangular carrier [13]. $G_d(s)$ represents the system delay, $G_c(s)$ is the transfer function of the outer loop controller. The proportional resonant (PR) regulator is introduced to eliminate the static error at the fundamental frequency. To simplify the analysis, the PR controller at fundamental frequency is given by:

$$G_c(s) = K_p + K_r \frac{2\omega_c s}{s^2 + 2\omega_c s + \omega_0^2} \quad (1)$$

where parameters K_p and K_r are the proportional and resonant gain, respectively. ω_0 is the fundamental angular frequency and ω_c is the bandwidth at -3 dB cutoff frequency. Generally, K_p determines the dynamic performance of the controller and affect the stability of the system, while K_r determines the gain at the selected frequency and controls the bandwidth around it.
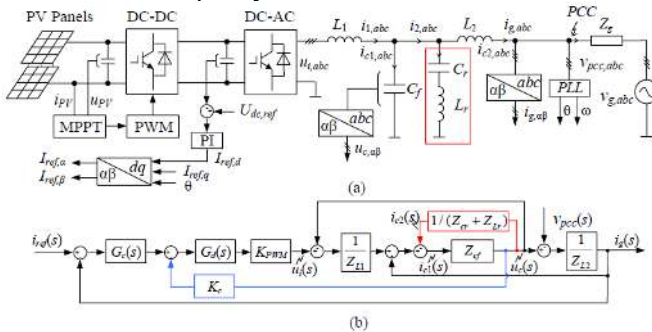

Fig. 1. Topology of a two-stage *LCL-LC* filtered grid-connected PV system (a) Main circuit (b) Control circuit
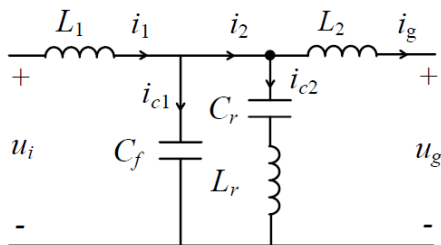

Fig. 2. Schematic diagrams of *LCL-LC* filter.

The *LCL-LC* filter is composed of a traditional *LCL* filter and a *LC* series resonant circuit as shown in Fig. 2. The transfer function from inverter output voltage u_i to injected grid current i_g is given as

$$G_{LCL-LC}(s) = \frac{s^2 L_r C_r + 1}{s^5 L_1 L_2 L_r C_r C_f + s^3(D_1 + D_2) + s(L_1 + L_2)} \quad (2)$$

where L_1 is the converter-side inductor, L_2 is the grid-side inductor. C_f is the filter capacitor, L_r is the resonant inductor and C_r is the resonant capacitor, and the terms in the denominator are defined as:

$$D_1 = L_1 L_2 (C_r + C_f) \ , \ D_2 = L_r C_r (L_1 + L_2) \quad (3)$$

The resonant frequency of the L_f-C_f series resonant circuit is at the switching frequency f_{sw}, thus the value of L_f is much smaller than that of L_1 or L_2. The main idea of designing the *LCL-LC* filter is to decompose the *LCL-LC* filter into a traditional *LCL* part and a *LC* series branch part. The parameters of the three-phase inverter system and the designed *LCL-LC* filter parameters are listed in Table I.

The f_{r1} and f_{r2} are the frequency where the two resonant peaks exist and they can be denoted as:

TABLE I   PARAMETERS OF THE THREE-PHASE INVERTER

Parameter	Symbol	Values
Line Voltage	E	110 Vrms
Rated Power	P	2.2 kW
Grid frequency	f_0	50 Hz
Switching frequency	f_{sw}	10 kHz
Sampling frequency	f_s	10 kHz
Modulation index	m	0.9
Dc-link voltage	U_{dc}	650 V
Inverter-side inductor	L_1	0.4 mH
Grid-side inductor	L_2	0.2 mH
Capacitor	C_f	12 uF
LC circuit inductor	L_r	21 uF
LC circuit capacitor	C_r	8 uF
First resonant frequency	f_{r1}	3.08 kHz
Second resonant frequency	f_{r2}	13 kHz
Grid-side inductor	L_2	0.2 mH

$$\begin{cases} f_{r1} = \sqrt{\dfrac{D_1 + D_2 - \sqrt{D_3 + D_4 + D_5}}{D_6}} \\[3mm] f_{r2} = \sqrt{\dfrac{D_1 + D_2 + \sqrt{D_3 + D_4 + D_5}}{D_6}} \end{cases} \quad (4)$$

where the parameters $D_3 \sim D_6$ are denoted as:

$$\begin{cases} D_3 = L_1^2 L_2^2 (C_r + C_f)^2 \\ D_4 = L_r^2 C_r^2 (L_1 + L_2)^2 \\ D_5 = 2 L_1 L_2 L_r C_r (L_1 + L_2)(C_r - C_f) \\ D_6 = 2 L_1 L_2 C_r C_f \end{cases} \quad (5)$$

To damp the resonance, the simplest way is to place a passive resistor in series or parallel with the inductor or capacitor of the *LCL-LC* filter. Generally speaking, when the damping resistor is in series with L_1 or L_2, the resonance at f_{r1} can be fully attenuated, but the resonance at f_{r2} cannot be fully eliminated, the damping effect of the resonance at f_{r2} increases with a larger damping resistor, but the gain at low frequency is also reduced.

III. ACTIVGE DAMPING METHOD FOR LCL-LC

Compared with passive damping methods, active damping strategy is more flexible and efficient, which adopts virtual resistor to eliminate power loss and can be easily incorporated into the existing control algorithm. Similar to traditional *LCL* filter, there are various feedback variables feasible for damping the resonance and stabilize the system, i.e., *LC* series branch voltage u_c, capacitor current i_{c1} and i_{c2}, and inverter side current i_1. And the current control diagrams are shown as Fig. 3.

Generally, the digital controlled system, contains the computation delay, sampler continuous approximation, and PWM delay. In the continuous domain, one-sample computation delay is expressed as

$$G_d(s) = e^{-s \cdot T_s} \qquad (6)$$

The zero-order hold (ZOH) introduces an extra delay of $0.5T_s$, which results in a total delay of $1.5T_s$ or $G_d(s)=e^{-s\lambda T_s}$ with $\lambda= 1.5$.

When the delay is considered, frequency f_R of capacitor current or *LC* series branch current feedback is smaller than that of capacitor voltage feedback. Therefore, in terms of closed-loop bandwidth, the proportional capacitor voltage feedback is preferred. However, a negative proportional gain K_{uc} is needed to stabilize the system.
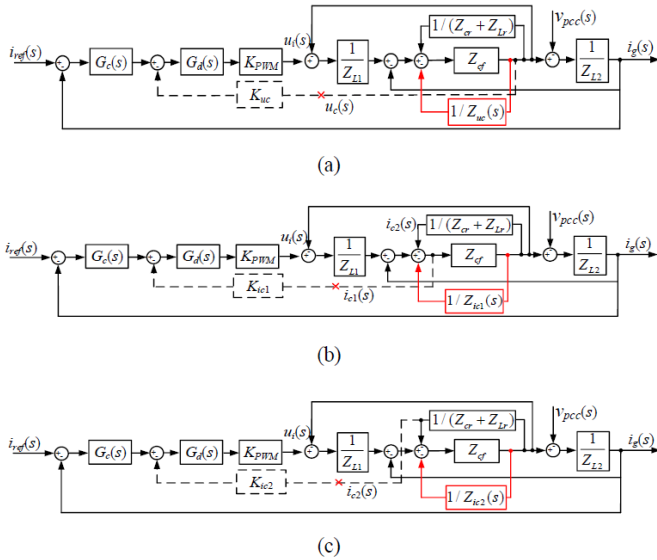

(a)

(b)

(c)

Fig.3. Current control using active damping method with (a) capacitor voltage u_c, (b) capacitor current i_{c1} and (c) *LC* circuit current i_{c2} feedback

IV. CONTROLLER DESIGN METHOD FOR LCL-LC FILTERED GRID-CONNECTED INVERTER

The control block diagrams of *LCL-LC* type grid-connected PV system with capacitor voltage feedback is shown in Fig. 1(a). To simplify the analysis, the grid current is expressed as

$$i_g(s) = \frac{G_L(s)}{1 + G_L(s)} i_{ref}(s) - \frac{G_b(s)}{1 + G_L(s)} v_g(s) \qquad (7)$$
$$= i_{g1}(s) + i_{g2}(s)$$

where the loop gain $G_L(s)$ can be expressed as

$$G_L(s) = \frac{G_c(s)G_d(s)K_{PWM}(1 + L_rC_r s^2)}{s^5 L_1 L_2 L_r C_r C_f + s^3 D_7 + s D_8} \qquad (8)$$

And the parameters in the denominator of (8) and $G_b(s)$ in (7) can be expressed as

$$D_7 = D_1 + D_2 + L_r C_r L_2 K_{uc} G_d(s) K_{PWM}$$
$$D_8 = K_{uc} G_d(s) K_{PWM} L_2 + L_1 + L_2 \qquad (9)$$

$$G_b(s) = \frac{Z_{L1} + Z_1}{Z_{L2}(Z_{L1} + Z_1) + Z_1 Z_{L1}}$$

where

$$\begin{cases} Z_1 = \dfrac{Z_{cf} Z_{uc}(Z_{cr} + Z_{Lr})}{(Z_{cf} + Z_{cr} + Z_{Lr})Z_{uc} + Z_{cf}(Z_{cr} + Z_{Lr})} \\ Z_{uc}(s) = \dfrac{sL_1}{K_{uc} G_d(s) K_{PWM}} \end{cases} \qquad (10)$$

The influence of the filter capacitor can be ignored when calculating the magnitude of the loop gain lower or equal to f_c. Thus $G_L(s)$ and $G_2(s)$ can be approximated as:

$$G_L(s) \approx T(s) = \frac{G_c(s)G_d(s)K_{PWM}}{s(K_{uc} G_d(s) K_{PWM} L_2 + L_1 + L_2)} \qquad (11)$$

$$G_b(s) \approx T_2(s) = \frac{(sL_1)^2 + K_{uc}(s)G_d(s)K_{PWM} sL_1 + sL_1}{s^3 L_2 L_1^2 + s^2(K_{uc}(s)G_d(s)K_{PWM} L_1 L_2 + L_1 L_2 + L_1^2)} \qquad (12)$$

The steady-state error of the grid-connected inverter includes the amplitude error E_A and the phase error δ. The PR controller can eliminate the static error at the fundamental frequency, thus the phase error δ can be minimized. Considering $T(s) \gg 1$ and $|G_d(j2\pi f_0)| \approx 1$, the amplitude of the grid current i_g at the fundamental frequency f_0 can be expressed as

$$i_g(j2\pi f_0) \approx i_{ref}(j2\pi f_0) - \frac{T_2(j2\pi f_0)}{T(j2\pi f_0)} v_g(s) \qquad (13)$$

and the amplitude error E_A can be expressed as

$$E_A = \frac{\left| |i_g(j2\pi f_0)| - i_{ref} \right|}{i_{ref}} \approx \left| \frac{1}{G_c(j2\pi f_0)} \right| \cdot \frac{V_g(K_{uc} + 1)}{I_{ref} K_{PWM}} \qquad (14)$$

where I_{ref} and V_g are the root mean square (RMS) values.

At the fundamental frequency f_o, the PR controller can be approximated as:

$$G_c(j2\pi f_0) \approx K_p + K_r \qquad (15)$$

Substituting (15) into (14) yields

$$K_{r\_EA} = \frac{V_g(K_{uc} + 1)}{E_A I_{ref} K_{PWM}} - K_p \qquad (16)$$

where K_{r_EA} is the critical value of the integral gain K_r constrained by E_A and K_{uc}. To ensure the system dynamic performance, the crossover frequency f_c is always set to be a value greater than 10 times over the fundamental frequency f_0. The magnitude of the PR controller can be approximated to K_p at the frequencies equal or higher than f_c, the magnitude frequency response of the system is zero at f_c. Therefore, considering $G_c(j2\pi f_c) \approx K_p$ and $|T(j2\pi f_c)| = 1$, the proportional gain K_p can be written as

$$K_P \approx \frac{2\pi f_c(K_{uc} K_{PWM} L_2 + L_1 + L_2)}{K_{PWM}} \qquad (17)$$

From (17), it can be inferred that K_p is proportional to f_c, and a larger K_p ensures a faster dynamic response. When the expected crossover frequency f_c and K_{uc} are selected, the proportional gain K_P can be determined.

As for *LCL-LC* filter, the phase curve crosses over -180° only at the second resonance frequency f_{r2}. Therefore, the gain at f_{r2} needs to be adjusted below 0 dB to ensure GM >0, and the resonant peak at f_{r2} needs to be effectively damped by tuning the active damping coefficient. Besides, the magnitude curve crosses over 0 dB at the cross over frequency f_c, the phase margin PM should also be higher than 0dB to ensure system stability.

As discussed earlier, the gain margin GM can be expressed as

$$\text{GM} = -20\lg|G_L(j2\pi f_{r2})| \qquad (18)$$

At the second resonance frequency f_{r2}, the influence of the filter capacitor is not negligible, considering $G_c(j2\pi f_{r2}) \approx K_p$, substituting $G_L(s)$ into (18), the boundaries of K_{uc} constrained by GM can be derived as (19), as shown at the bottom of this page.

The PM of the system can be expressed as

$$\text{PM} = 180° + \angle G_L(s)|_{s=j2\pi f_c} \qquad (20)$$

To calculate the phase margin, using $G_c(j2\pi f_c) \approx K_p+2K_r$ is more accurate. Substituting s = $j2\pi f_c$ into $G_L(s)$ in (20), the PM can be rewritten as

$$\text{PM} = -180^0 + \arctan\frac{K_p\pi - 4\pi^3 K_p L_r C_r}{K_r\omega_c - 4\pi^2 K_r\omega_c L_r C_r} \qquad (21)$$

According to (21), K_r can be expressed as

$$K_r = \frac{\pi K_P - 4\pi^3 K_P L_r C_r}{\tan(\text{PM}+180°)(\omega_c - 4\pi^2\omega_c L_r C_r)} \qquad (22)$$

Substituting (16) and (17) into (22), the proportional damper K_{uc} constrained by PM and E_A can be derived as

$$K_{uc\_PM} = \frac{G_{EA}K_{PWM}G_d(s) - V_g G_{PM} + G_{EA}2\pi f_c(L_1+L_2)}{(V_g G_{PM} - G_{EA}2\pi f_c K_{PWM}G_d(s)L_2)} \qquad (23)$$

where the G_{PM} and G_{EA} is related to the specified phase margin PM and the amplitude error E_A, respectively, which is shown in (24)

$$\begin{cases} G_{PM} = \tan(\text{PM}+180^0)(\omega_c - 4\pi^2\omega_c L_r C_r) \\ G_{EA} = E_A I_{ref}(\pi - 4\pi^3 L_r C_r) \end{cases} \qquad (24)$$

From the above analysis, it can be seen that if the upper and lower boundaries of GM and PM, and E_A are specified, the satisfactory region constrained by K_{uc} and f_c can be obtained from (19) and (23). From Fig. 4, the crossover frequency f_c and the proportional damper K_{uc} can be easily selected. Then, with the possible value of f_c and K_{uc}, the proportional gain K_P can be calculated from (17), the relationship between K_p, K_{uc} and f_c is plotted in Fig. 5. Generally, a larger f_c is always selected to ensure good dynamic response, thus the area for satisfactory range of K_p are depicted in the shaded area in Fig. 5. Finally, with the obtained K_p and K_{uc}, the integral gain K_r

can be calculated from (16), and the relationship between K_r, K_{uc} and K_p is plotted in Fig. 6. As can be seen, a bigger K_r is required to reduce the amplitude error E_A, and the area for satisfactory range of K_r is depicted in the shaded area with better dynamic and less steady-state error.

To verify the design method, an example is given. If the upper and lower boundaries of PM and GM is chosen as 30° ≤ PM ≤ 60° and 3 dB ≤ GM ≤ 12 dB, respectively, which ensure good dynamic performance and stability margin. Besides, the magnitude error E_A is expected to be less than 0.4%. Based on (19) and (23), the satisfactory region constrained by K_{uc} and f_c can be obtained. From Fig. 4, point A is selected with f_c = 2150 Hz and K_{uc} =-0.28. With (17), the calculated proportional gain K_p is 0.49. Substituting K_{uc}, K_p and E_A into (16), K_r=40 can be obtained. Considering the previous steps, the designed parameters can be defined as:

$$K_p = 0.49, K_r = 40, K_{uc} = -0.28 \qquad (25)$$

Based on the designed parameters, the system bode diagram with compensation is shown in Fig 7. The gain margin (GM) is 5.21 dB, the phase margin (PM) is 43° and the crossover frequency f_c is 2.15 kHz. Therefore, both the dynamic performance and stability of the *LCL-LC* filter interfaced PV system are achieved.
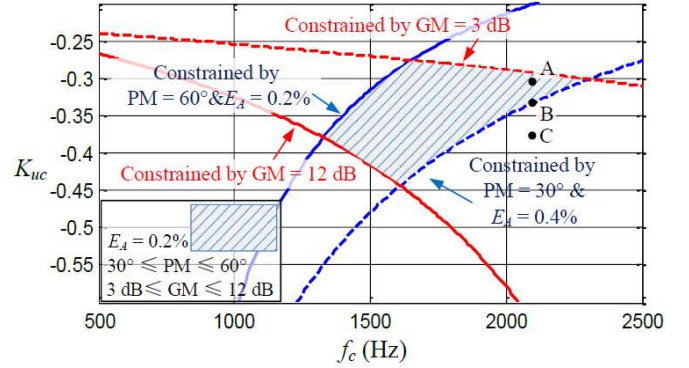

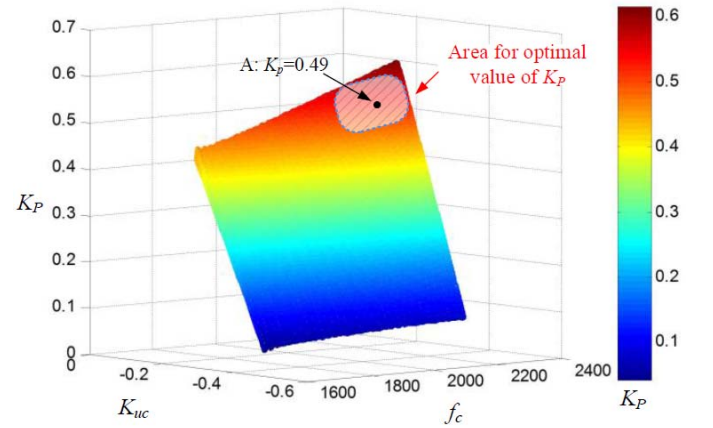Fig. 4. Region of f_c and K_{uc} constrained by GM PM and E_A.

Fig. 5. Relationship between K_p, K_{uc} and f_c.

$$K_{uc\_GM} = \frac{32\pi^5 f_{r2}^5 C_f C_r L_r L_1 L_2 + 2\pi f_c(L_1+L_2)(4\pi^2 f_{r2}^2 L_r C_r - 1)10^{\frac{GM}{20}} - 8\pi^3 f_{r2}^3(G_1+G_2) + 2\pi f_{r2}(L_1+L_2)}{2\pi f_c K_{PWM}G_d(s)L_2(1-4\pi^2 f_{r2}^2 L_r C_r)10^{\frac{GM}{20}} + 8\pi^3 f_{r2}^3 L_r C_r K_{PWM}G_d(s)L_2 - 2\pi f_{r2}K_{PWM}G_d(s)L_2} \qquad (19)$$
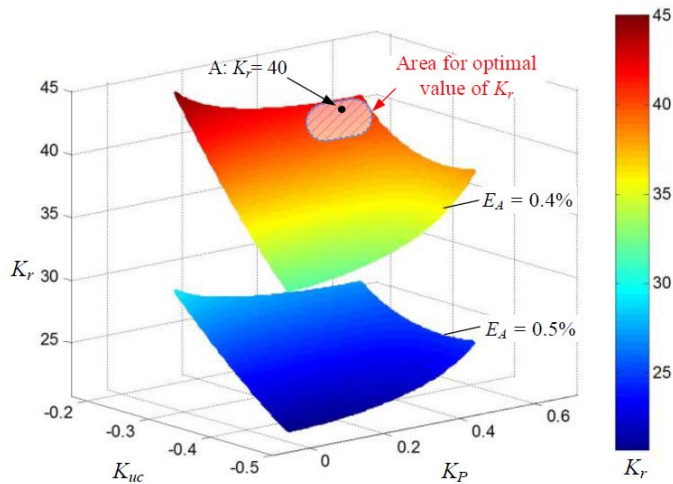
Fig. 6. Relationship between K_r, K_{uc} and K_P with different E_A.

V. SIMULATION RESULTS AND DISSCUSSION

A detailed model of the *LCL-LC* grid-connected PV system in Fig. 1 is implemented in Matlab/Simulink to verify the theoretical analysis, and the *LCL-LC* parameters are listed in Table I.
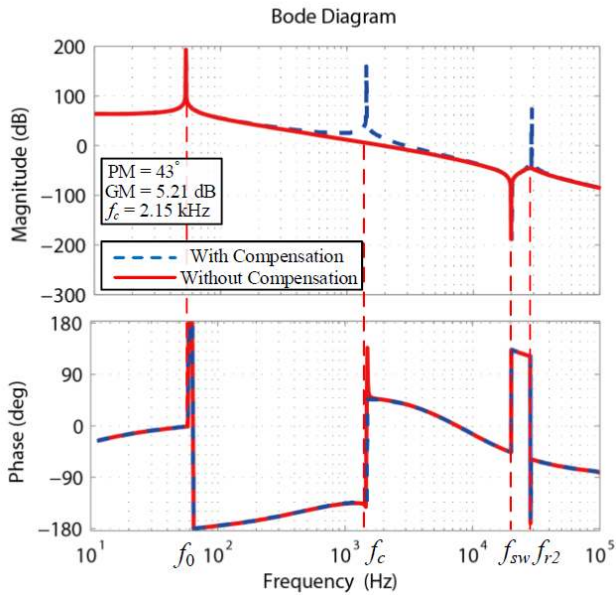

Fig. 7. Bode diagrams of the compensated $G_L(s)$.

In weak grid scenario, the grid impedance is inductive and can be regarded as equivalent to the increasing of inductor L_2. In this experimental study, L_2 is increased by 60% and 120% its value to simulate the weak grid condition. As can be seen in Fig. 8(a), when the inductor L_2 is increased by 60%, the system is stable with low distortion in grid currents. With larger value of L_2 in Fig. 8(b), the THD is increased and the system is still stable. Moreover, if L_2 is decreased by 20%, as shown in Fig. 8(c), the overshoot is increased but the system stability is still not affected. Thus the effectiveness of the *LCL-LC* grid-connected system against the grid impedance variation is confirmed.
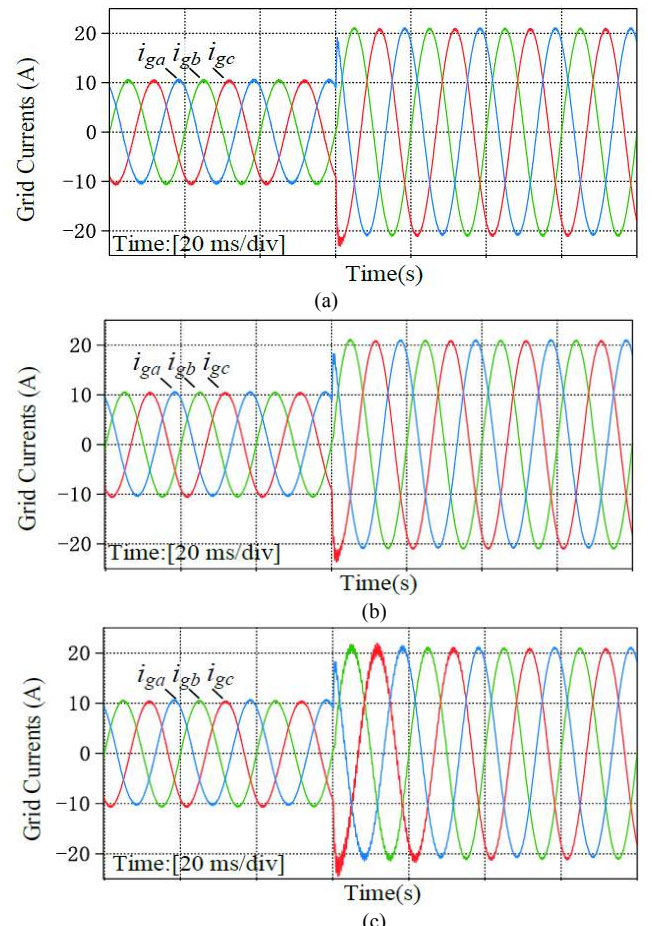

Fig. 8. Experimental waveforms of *LCL-LC* filter with the variation of inductor L_2: (a) Inductor L_2 increased by 60%, (b) Inductor L_2 increased by 120% and (c) Inductor L_2 decreased by 20%.
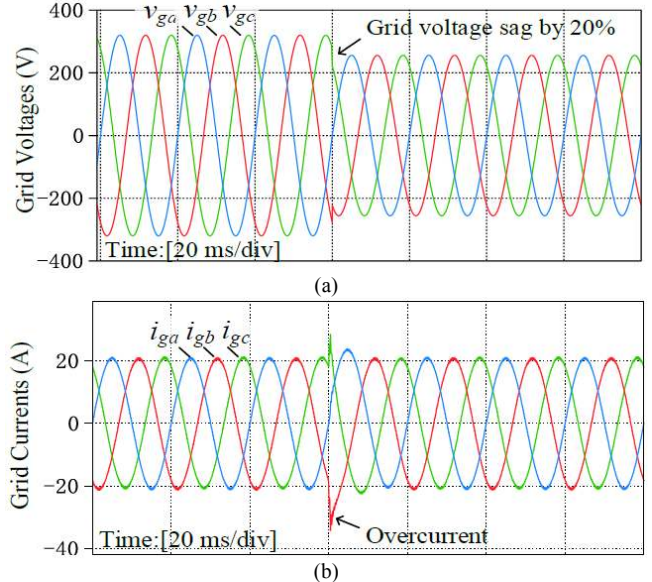

Fig. 9. Simulation results with grid voltages decreased by 20%: (a) Grid voltages and (b) Grid currents.

In order to integrate into the grid properly, the PV power plants must be robust enough against the grid voltage fluctuation. In this study, grid voltages are decreased by 20%

to simulate the grid voltage sag and swell situation. As can be seen in Fig. 9(a), if the grid voltages decrease by 20%, the system is stable with small overcurrent at the transition point.

To emulate the grid voltage distortion phenomena, the supply voltage is distorted with 2% fifth, 1.5% seventh and 1% eleventh harmonics with respect to the grid fundamental voltage. As shown in Fig. 10(a), the measured total harmonic distortion (THD) of the grid voltages is 2.82%, and the grid currents are significantly distorted in Fig. 10(b). To restrain the distortion of the grid currents, the PR plus harmonic compensator (PR+HC) structure is adopted. In Fig. 10(c), When PR+HC controller is used, the grid currents waveforms are quite sinusoidal and the THD is only 4.28%. It's illustrated that the designed *LCL-LC* grid- connected PV system with capacitor voltage feedback scheme has a strong robustness against the grid impedance variations.
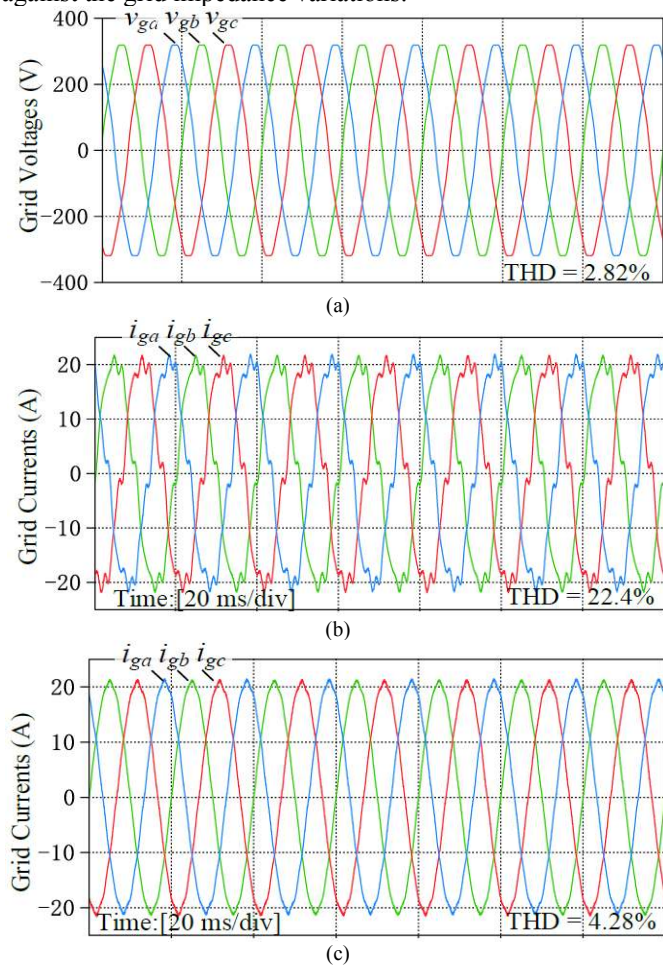

Fig. 10. Simulation results under distorted grid voltages: (a) Grid voltages (b) Grid currents with PR controller and (c) Grid currents with PR+HC controller.

VI. CONCLUSION

This paper investigates the passive damping methods for the *LCL-LC* filter interfaced grid-connected PV inverters. And on this basis, the active damping method is proposed with wider system bandwidth by using capacitor voltage feedback. Taking into account the effect of the control delay, this paper presents a systematic parameter design method for *LCL-LC*

filtered grid-connected PV system. With this method, controller parameters and the active damping feedback coefficient can be easily obtained by specifying system stability and dynamic performance indices, and it is more convenient to optimize the system performance according to the predefined satisfactory region. The simulation results are presented and verified that the designed *LCL-LC* grid-connected system with capacitor voltage feedback has strong robustness against the grid impedance variations and the grid voltage fluctuations.

REFECENCE

[1] A. Honrubia-Escribano, Garci, x, S. a, x, T. nchez, *et al.*, "Power quality surveys of photovoltaic power plants: characterisation and analysis of grid-code requirements," *Renewable Power Generation, IET,* vol. 9, pp. 466-473, 2015.

[2] Y. Han, M. Luo, X. Zhao and J.M. Guerrero, "Comparative performance evaluation of orthogonal-signal-generators-based single-phase PLL algorithms—a survey," *IEEE Trans. Power Electron.,* vol.31, no.5, pp.3932-3944, Aug. 2015.

[3] Y. Han, M. Luo and J.M. Guerrero, "Dynamics assessment of grid-synchronization algorithms for single-phase grid-connected converters," 9th International Conference on Power Electronics – ECCE Asia, 2015, pp. 1228-1233.

[4] M. Huang, X. Wang, P. C. Loh, and F. Blaabjerg, "LLCL-Filtered Grid Converter with Improved Stability and Robustness," *Power Electronics, IEEE Transactions on,* vol. PP, pp. 1-1, 2015.

[5] W. M. Wu, Y. B. He, T. H. Tang, and F. Blaabjerg, "A New Design Method for the Passive Damped LCL and LLCL Filter-Based Single-Phase Grid-Tied Inverter," *IEEE Trans. Ind. Electron.,* vol. 60, pp. 4339-4350, Oct 2013.

[6] Y. Liu, W. Wu, Y. He, Z. Lin, F. Blaabjerg, and H. S. H. Chung, "An Efficient and Robust Hybrid Damper for LCL- or LLCL-based Grid-Tied Inverter with Strong Grid-side Harmonic Voltage Effect Rejection," *Industrial Electronics, IEEE Transactions on,* vol. PP, pp. 1-1, 2015.

[7] L. Fei, Z. Xing, Z. Hong, L. Haoyuan, and Y. Changzhou, "An LCL-LC Filter for Grid-Connected Converter: Topology, Parameter, and Analysis," *Power Electronics, IEEE Transactions on,* vol. 30, pp. 5067-5077, 2015.

[8] M. Huang, X. Wang, P. C. Loh, and F. Blaabjerg, "Active Damping of LLCL-Filter Resonance Based on LC-Trap Voltage or Current Feedback," *Power Electronics, IEEE Transactions on,* vol. PP, pp. 1-1, 2015.

[9] Y. Han, Z. Li, and J. M. Guerrero, "Dynamic evaluation of LCL-type grid-connected inverters with different current feedback control schemes," in *Power Electronics and ECCE Asia (ICPE-ECCE Asia), 2015 9th International Conference on*, 2015, pp. 391-396.

[10] H. Min, F. Blaabjerg, and L. Poh Chiang, "The overview of damping methods for three-phase grid-tied inverter with LLCL-filter," in *Power Electronics and Applications (EPE'14-ECCE Europe), 2014 16th European Conference on*, 2014, pp. 1-9.

[11] L. Yi, X. Wei, M. Chaoxu, Z. Zhengming, L. Hongbing, and L. Zhiyong, "New Hybrid Damping Strategy for Grid-Connected Photovoltaic Inverter With LCL Filter," *IEEE Trans. Applied Superconductivity,* vol. 24, pp. 1-8, 2014.

[12] C. Tang, Y. Chen, and Y. Chen, "PV Power System With Multi-Mode Operation and Low-Voltage Ride-Through Capability," *Industrial Electronics, IEEE Transactions on,* vol. 62, pp. 7524-7533, 2015.

[13] C. L. Bao, X. B. Ruan, X. H. Wang, W. W. Li, D. H. Pan, and K. L. Weng, "Step-by-Step Controller Design for LCL-Type Grid-Connected Inverter with Capacitor-Current-Feedback Active-Damping," *IEEE Trans. Power Electron.,* vol. 29, pp. 1239-1253, Mar 2014.